J. Low Power Electron. **2013**, *3*, 279-299; doi:10.3390/jlpea3030279

OPEN ACCESS
Journal of
Low Power Electronics and Applications
ISSN 2079-9268
www.mdpi.com/journal/jlpea

Article

Low-Gain, Low-Noise Integrated Neuronal Amplifier for Implantable Artifact-Reduction Recording System

Adeline Zbrzeski [1,2,3,*], Noëlle Lewis [2,3], Francois Rummens [2,3], Ranu Jung [1], Gilles N'Kaoua [2,3], Abdelhamid Benazzouz [4] and Sylvie Renaud [2,3]

1 Department of Biomedical Engineering, Florida International University, Miami, FL, 33174, USA
2 University of Bordeaux, Laboratoire de l'Integration du Materiau au Systeme, UMR 5218, Talence, France; E-Mail: rjung@fiu.edu
3 CNRS, Laboratoire de l'Integration du Materiau au Systeme, UMR 5218, Talence, France; E-Mails: noelle.lewis@ims-bordeaux.fr (N.L.); francois.rummens@etu.enseeiht.fr (F.R.); gilles.nkaoua@ims-bordeaux.fr (G.N.); sylvie.renaud@ims-bordeaux.fr (S.R.)
4 University of Bordeaux, Institute of Neurodegenerative Diseases, UMR 5293, Bordeaux, France; E-Mail: abdelhamid.benazzouz@u-bordeaux2.fr

* Author to whom correspondence should be addressed; E-Mail: azbrzesk@fiu.edu; Tel.: +1-305-348-4781; Fax: +1-305-348-6954.

Received: 6 March 2013; in revised form: 8 July 2013 / Accepted: 6 August 2013 / Published: 9 September 2013

Abstract: Brain neuroprostheses for neuromodulation are being designed to monitor the neural activity of the brain in the vicinity of the region being stimulated using a single macro-electrode. Using a single macro-electrode, recent neuromodulation studies show that recording systems with a low gain neuronal amplifier and successive amplifier stages can reduce or reject stimulation artifacts. These systems were made with off-the-shelf components that are not amendable for future implant design. A low-gain, low-noise integrated neuronal amplifier (NA) with the capability of recording local field potentials (LFP) and spike activity is presented. *In vitro* and *in vivo* characterizations of the tissue/electrode interface, with equivalent impedance as an electrical model for recording in the LFP band using macro-electrodes for rodents, contribute to the NA design constraints. The NA occupies 0.15 mm^2 and dissipates 6.73 µW, and was fabricated using a 0.35 µm CMOS process. Test-bench validation indicates that the NA provides a mid-band gain of 20 dB and achieves a low input-referred noise of 4 μV_{RMS}. Ability of the NA to perform spike recording

in test-bench experiments is presented. Additionally, an awake and freely moving rodent setup was used to illustrate the integrated NA ability to record LFPs, paving the pathway for future implantable systems for neuromodulation.

Keywords: low-noise amplifier; front-end; macro-electrode; neuralrecording; neuromodulation

1. Introduction

Monitoring brain neural activity in the vicinity of a region being stimulated for active neuromodulation is used in various applications such as deep brain stimulation [1,2] and epilepsy [3]. Developments of such closed-loop systems (Figure 1) have to address limitations in our understanding of the pathophysiological changes in brain function following implantation as well as several electrical engineering challenges. In these neuromodulatory applications, it is first necessary to record a neural signal that reflects ongoing neuronal activity. This neural biomarker could be used as an input to the closed-loop system for real-time automatic modification of the stimulation parameters for neuromodulation.

Figure 1. Schematic representation for a future implantable closed-loop real-time neuroprosthesis for neural stimulation.

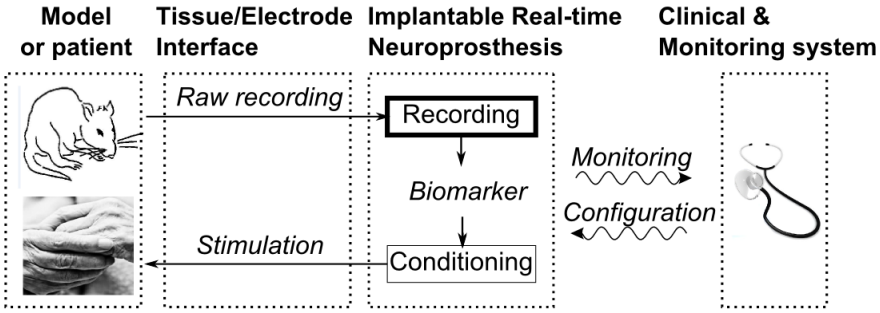

A single macro-electrode provides both recording and stimulation of neuronal activity from surrounding brain tissue. The raw neuronal recording provides a biomarker signature. Its detection could control the stimulation patterns in order to improve the stimulation therapeutic impact.

Various features of neuronal activity in Parkinson's disease may act as biomarkers for closed-loop control. Single-unit spike patterns of neural firing recorded in the vicinity of the stimulated area could act as biomarkers of the ongoing neuronal activity. On the other hand, local field potential signals (LFPs) that reflect the activity of a population of cells (hundred or more cells) could also act as potential biomarkers and have been used for a broad range of closed-loop applications and can be used in a closed-loop system [4]. While external systems have been developed to record spikes or LFPs for use in closed-loop systems [3,5,6], the design and validation of an implantable spike and LFP recording amplifier that could overcome the problems associated with stimulation in close vicinity of the recording electrode are yet to be addressed. Here, we present the design and prototype fabrication of a low gain, integrated neuronal amplifier for recording spikes and LFPs to address this challenge.

In order to design and to determine the size of the input impedance of the amplifier of the recording circuit, it is essential to characterize the tissue/electrode interface. The tissue/electrode interface is usually characterized by an equivalent impedance for the frequency band from 100 Hz to several kilo-Hertz which does not capture the low-frequency bandwidth of interest for LFPs, or as an "equivalent resistance" at 1 kHz [7]. If the same electrode is used for stimulation and recording (e.g. [6,8,9]), a macro-electrode is used (equivalent resistance in the order of hundreds of kilo-Ohm) instead of a micro-electrode. Because of its large area, such a macro-electrode is likely to pre-dominantly record extracellular LFPs. For purposes of stimulation, previous studies have characterized on the LFP and spike bands large, four-contact macro-electrodes such as those used for deep brain stimulation in *in vivo* large animal studies [10,11]. For targeting smaller brain areas or for use in laboratory research in small animals, smaller macro-electrodes have to be utilized [12].

The overall engineering challenge we have addressed is the design for a future implantable recording system that is able to appropriately condition the neuronal signal to facilitate detection of an identified biomarker within a closed-loop configuration. The circuitry for neuronal recordings should satisfy three key engineering specifications (Table 1).

Table 1. Neural recording characteristics and requirements, with associated neuronal amplifier specifications.

Feature	**Requirements**	**Specifications**
Macro-electrode	Tissue/macro-electrode model on LFP band (NEX100)	*No in vivo data*
Engineering Challenges	Compliant with an closed-loop system using a single electrode (stimulation artifact)	Recording circuit strategy
	Low power	≥10 μW
	Low area	≥0.2 mm^2
	Noise	5 μV_{RMS}
***In vivo* biosignal**	**Characteristics**	**Range**
LFP	Band	1–300 Hz
	Amplitude	10 μV–1 mV
Spike	Band	300Hz–10 kHz
	Amplitude	10 μV–1 mV

First, if a single electrode has to be used for recording and stimulation because of anatomical constraints or to avoid two separate surgical implantations, the recording circuitry must be able to attenuate the electrical stimulation artifact. This signal should not saturate the NA. This requirement can be addressed by use of an appropriate recording circuit strategy, detailed in section II. Briefly, this recording strategy for closed-loop systems consists of cascading, low-gain, and second-order filter amplifier stages. Although some systems have previously been successfully validated *in vivo*, they use commercial off-the-shelf (COS) components which are not amenable to future implantation. Moreover, none of the studies published in the literature have reported tissue/electrode matching, noise quantification and/or characterization of the neuronal amplifier. Second, the circuit design must meet low-power and low-area specifications to be readily integrated into an overall circuit design amenable to long-term implantation. This can be accomplished by use of an integrated system that includes mixed analog and digital components. Third, the recording circuitry will require a neuronal amplifier

with low intrinsic noise that does not override the low amplitude of the recorded neuronal signal and amplifies it sufficiently to be above the noise floor of the cascading circuits of the closed-loop recording system. The noise requirement is particularly challenging for LFP recordings because the LFP band (from DC to ~300 Hz) is close to significant 1/f and popcorn noise in transistors [13].

Finally, experimental validation is necessary to assess the usability of the circuitry through test-bench and *in vivo* experiments. Although the LFPs are the primary signals of interest, the NA should also provide the opportunity to record spike signals for other closed-loop paradigm validations.

This original work presents the full design methodology of a low noise low gain amplifier, taking into account the *in vivo* environment along the entire flow. The work presents three key features: (1) *in vitro* and *in vivo* characterizations of the tissue/electrode interface (equivalent impedance) for LFP recording using macro-electrodes for rodents, which complete missing specification for the design of the neuronal amplifier (NA); (2) the design and prototype fabrication of a low gain, integrated neuronal amplifier for recording spikes and LFPs for the aforementioned close-loop recording strategy cascading architecture, meeting low noise, area and power performances for amenable future implantation; and (3) experimental demonstration of the ability of the NA to record spikes (test-bench) and LFPs (*in vivo* experiments) with detailed description of the experimental setup and procedures for LFP and spike recording design methodology and validation that have previously not been explicitly published in the literature.

2. Design Methods

2.1. Specifications

2.1.1. Biosignal Characteristics

Recordable neuronal activity includes LFPs and spikes. Each type of neuronal activity is characterized by its band and dynamic range (Table 1, [13–15]). The LFP and spike band corners can vary depending on the application. The intermediate frequency between these bands is typically in the order of hundreds of hertz, and the spike highest corner is usually defined in the 5–10 kHz range. The dynamic range depends on the recording measurement techniques (intra- or extracellular), as well as the electrode equivalent impedance. Our area of interest is implanted recording systems that use extracellular macro-electrodes.

2.1.2. Tissue/Macro-Electrode Interface Characterization

As defined in the introduction, in this study we report the characterization of the *in vitro* and *in vivo* tissue/electrode interface equivalent impedance for macro-electrodes for recording in the LFP band in rodent. As further detailed in the Results section, the tissue/electrode electrical model of the rodent macro-electrode is equivalent to a capacitor C_e in the LFP band and to a resistor in the spike band. This equivalent model has an impact on the NA design sizing.

2.1.3. Neuronal Amplifier Topology for Recording Circuit Strategy Used in Closed-Loop System for Artifact Rejection

To our knowledge, two main recording circuit strategies have been used for closed-loop systems using a single electrode and for possible integration on chip for implantable systems. These strategies, described below, lead to different NA topology designs.

The NA could rely on a mixed-signal topology based on a heterodyning method coupled with a chopper-stabilization technique to minimize 1/f noise and DC stabilization initially introduced by Dagtekin *et al.* [16]. One of the most advanced closed-loop integrated designs in our context was presented by Denison *et al.* [9,13]. Denison *et al.* designed the recording system assuming that the biomarker and the stimulation bands were well separated. This recording circuit strategy was validated within a closed-loop system by controlling epileptic activity in the brain in a large animal model [9]. The main drawback of this topology is the area consumption, which is 0.7 mm^2 without the required ~1 mm^2/input capacitor.

Another recording circuit strategy for use in closed-loop systems is cascading, low-gain, second-order filter amplifier stages (*i.e.*, high gain, high-order overall filter). Validation of this strategy was demonstrated by recording and stimulation of neuronal activity by Rossi *et al.* in the subthalamic nucleus (STN) of two idiopathic PD patients [6], and by Kent and Grill [8] in the ventral lateral thalamus of an adult cat. Despite successful *in vivo* recording circuit strategy validation within a closed-loop system, both authors used commercial off-the-shelf (COS) components to implement the neuronal amplifier, *i.e.*, the NA is not amenable to implantation because of high power and area consumptions. Moreover, no noise quantification and/or characterization of the neuronal amplifier were reported in either study.

2.1.4. Integrated Neuronal Amplifier Specifications

Based on the biosignal characteristics outlined in the first sub-section, we specified the bandwidth of the neuronal amplifier to be 1 Hz–10 kHz and the dynamic amplitude range to be 10 μV–100 mV since the NA should be able to record both LFPs and spikes.

Based on the tissue/macro-electrode interface characterization outlined in the second sub-section, the equivalent input impedance of the NA should be appropriately sized by taking into account the equivalent implanted macro-electrode impedance and its value.

Additionally, the NA specifications depend on the NA topology for recording appropriate signals for an implantable closed-loop system using a single electrode. To address this requirement, we designed an integrated NA compliant with the recording topology based on cascading low gain second-order filter amplifier stages [6,8]. We chose to set the neuronal amplifier gain to be 20 dB to help prevent saturation. This low gain value is compliant with settings used for the *in vivo* recording circuit strategy validation [6,8].

Therefore, the engineering challenge of the design was to meet the noise requirement over LFP and spike bands with a low NA gain over the bands and with power and area specifications compliant with future implementation in an integrated neuroprosthesis system. The power consumption (no more than

10 μW) and the area consumption (no more than 0.2 mm^2) were set to be in the same order as that of high gain NAs previously described in the literature [17–19].

2.2. Design of the Integrated Neuronal Amplifier

2.2.1. Integrated Neuronal Amplifier Topology

Figure 2a presents the topology for the neuronal amplifier used for this work, initially presented for neural recoding by Harrison *et al.* [20]. This NA filters and amplifies the input signal. The transfer function $H_{NA}(p)$, gain A_v and low and high cut-off frequencies f_{low} and f_{high} of the NA are defined in Equations (1) and (2).

$$H_{NA}(p) = Av.\frac{1-\frac{p}{2.\pi.f_z}}{\left(1+\frac{2.\pi.f_{low}}{p}\right).\left(1+\frac{p}{2.\pi.f_{high}}\right)} \quad (1)$$

$$A_v = \frac{C_1}{C_2};\ f_{low} = \frac{1}{2.\pi.R_2.C_2};\ f_{high} = \frac{G_m}{2.\pi.C_L.A_v} \quad (2)$$

with f_z: the zero frequency; G_m: the transconductance of the operational transconductance amplifier (OTA); and C_L: the load capacitor of the neuronal amplifier. Proper sizing of the different components of this topology were selected to meet the electrical specifications.

Figure 2. Neuronal amplifier (**a**) Topology with the resistor R_2 implemented with a MOS-bipolar pseudo-resistor R_2; (**b**) Low noise operational transconductance G_m amplifier topology with: I_{bias} the bias current, V_{in+} and V_{in-} the voltage inputs, V_{out} the voltage output, V_{pol} the tunable voltage, and V_{dd}/V_{ss} the power supply.

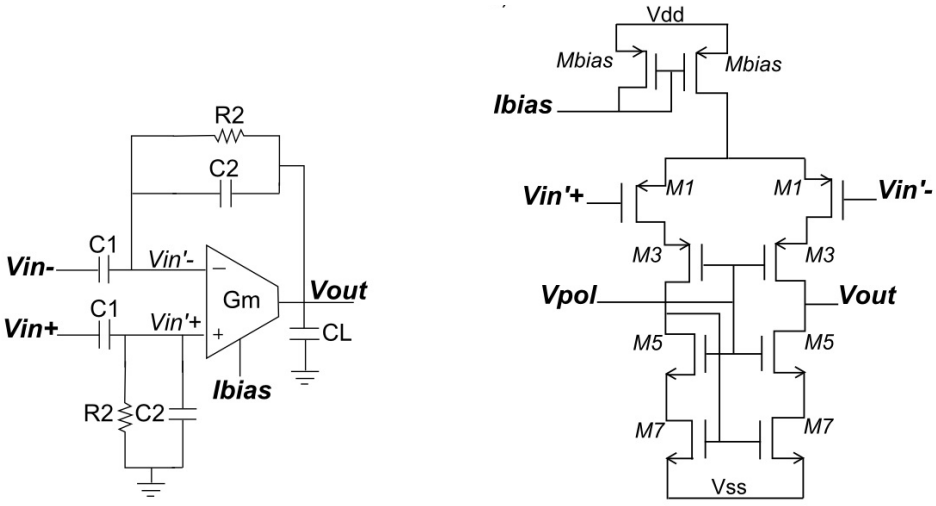

(**a**) (**b**)

2.2.2. Sizing Procedure and Layout Considerations

Several neuronal amplifier design techniques implement R_2 as an integrated resistance as discussed in [21,22]. We used a lateral PNP for R_2, which is equivalent to a MOS-bipolar pseudo-resistor [23] but presents smaller noise contribution according to our simulations. It essentially works as a

diode-connected PMOS transistor for negative gate source voltage V_{gs} and a parasitic PNP transistor for positive V_{gs}.

The capacitors' (C_1 and C_2) values were chosen based on three criteria: the impact of the electrode model on the NA design, stability, and specification requirements (gain and low cut-off frequency). First, the capacitor C_1 is limited because of its silicon area cost. The equivalent NA input model consists of a series of the tissue/macro-electrode 34 nF-C_e capacitor (see results section) with the NA input C_1 capacitor. The C_1 capacitor should be low enough in comparison to the tissue/macro-electrode capacitor C_e to avoid input signal attenuation. Second, the pole frequency f_z should be pushed to high values to ensure stability, which implies $\sqrt{C_1.C_L}$ is significantly larger than C_2. Electrical specifications define the bandpass filter parameters. The definition of R_2 dictates the C_2 sizing in reference to the low cut-off frequency f_{low}. Moreover, our neuronal amplifier design differs from others in that it uses a low gain. Although a high gain decreases the influence of the noise of subsequent stages, we limited it to 20dB as stated in the electrical specifications. Using Cadence simulations to evaluate performance and tradeoffs, we chose the following component values: C_1 = 45 pF, C_2 = 4.5 pF, C_L = 8 pF, R_2 = 35.3 GΩ, G_m = 5.02 µS.

The neuronal amplifier OTA architecture was then chosen. The following are the commonly used OTA architectures: symmetrically balanced, Miller, telescopic and folded-cascode structures. Our design uses a telescopic, or single-stage cascode, topology which offers one of the best noise-power trade-offs [24]. The thermal and flicker noise minimization is mainly achieved by the input differential pair design: large PMOS transistors are used instead of NMOS because their technological manufacturing process results in lower flicker noise and a moderate inversion region is used based on the MOSFET operating plane [25]. The OTA topology is presented in Figure 2b. Mismatch and process variation can be reduced by means of appropriate layout techniques such as interdigitated structures and common-centroid configurations for careful matching of MOS NA input differential pairs and current mirrors. The use of these techniques minimizes the comparator offset voltage.

The neuronal amplifier overall noise on the 1–10 kHz band is composed of dominant R_2 noise (or flicker noise) from 1 Hz to f_{corner} and dominant OTA noise from f_{corner} to 10 kHz. The design should consider the limit frequency f_{corner} defined in Equation (3) [26]. We simulated the neuronal amplifier's overall noise and estimated f_{corner} to be 10Hz.

$$f_{corner} \approx \sqrt{f_{low} \cdot f_{high} \cdot \frac{3.C_L}{2.C_1}} \tag{3}$$

With the above stated design considerations, an integrated circuit was designed and fabricated using the AMS 0.35 µm CMOS process from Circuits Multi-Projects (Grenoble, France). A die photograph of the NA in the integrated circuit is shown in Figure 3. Other functions were also designed on the same integrated circuit, including filtering functions and are discussed in [27].

Figure 3. (**a**) Photomicrograph of the AMS 0.35 μm CMOS prototype integrated circuit including the neuronal amplifier; and (**b**) detail of the neuronal amplifier layout. The neuronal amplifier components described in the schematic in Figure 2a are identified in Figure 2b. The neuronal amplifier area is 0.15 mm^2, including 0.012 mm^2 for the integrated capacitors and 0.0019 mm^2 for the operational transconductance amplifier.

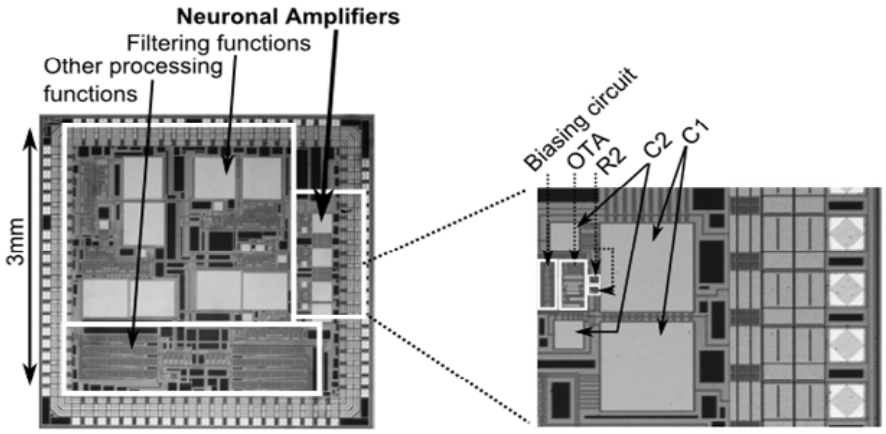

(**a**) (**b**)

3. Validation Methods

Three performance measurements were utilized for validating the design of the integrated neuronal amplifier. First, the tissue/macro-electrode interface model was characterized on the LFP band from *in vitro* and *in vivo* measurements. Then, the neuronal amplifier electrical performances were characterized with test-bench experiments. Finally, test-bench and awake animal experiments demonstrated the NA recording functionality. The setups for these experiments are described in this section. The developed test-bench for the electrical characterization and test-bench validation is also described.

3.1. Animal Preparation

Electrophysiological recordings were conducted for the tissue/macro-electrode electrical model and NA functionality experiments on eight adult male Sprague-Dawley rats weighing 460 ± 151 g. Surgical and experimental procedures were performed in accordance with the European Community's Council Directive (EU Directive 2010/63/EU) and the National Institute of Health Guide for Care and Use of Laboratory Animals. A concentric bipolar stimulation electrode (NEX100, Phymep, France) was implanted in the right STN of the brain using stereotaxic procedures according to the atlas of Paxinos and Watson (1986) [28].

Electrophysiological recordings of neuronal signals were done under two conditions: animal under anaesthesia (terminal acute study) or awake and freely moving (acute study). The tissue/macro-electrode electrical model characterization used three anesthetized animals. The NA functionality was first assessed with an anesthetized animal but the *in vivo* recording setup required improvements to avoid punctate excessive 50 Hz power line interference (Section 4.4). After improving the *in vivo* recording

setup, NA functionality was assessed in two anesthetized animals and three animals under awake conditions (one animal was used for recording under both conditions).

Spontaneous recordings under the first condition were made under anaesthesia induced using urethane (10 mL/kg). In order to record LFP signals in freely moving conditions, animals were implanted with a chronic stimulating electrode in the right STN under anaesthesia with a 1.9 $mg.kg^{-1}$ solution of 52% ketamine (Virbac, France), 22% xylazine (Rompun, Bayer Vital, Germany) and 26% saline solution (B. Braun, France). Body temperature was maintained at 37 °C ± 0.5 S.D. with the use of a homeothermic heating blanket. *Cortanmycétine* cream (Intervet, France) was applied to the eyes to prevent corneal dehydration and infection. Rats were placed in a stereotaxic frame and a craniotomy was performed over the right STN (AP: −3.8, ML: 2.5) according to the rat brain atlas [28]. Six screws were placed around the craniotomy (A2 DIN 84, Fixnvis, France) and covered with dental composite resin (SuperBond C&B, Sun Medical, Japan). A bipolar electrode (MS306/SP, PlasticsOne, USA) was then lowered into the perforation to a depth of 8 mm below the cortical surface. The electrode base and screws were finally covered with dental cement (Dentalon Plus, HeraeusKulzer, USA). After suturing, wounds were infiltrated with analgesic (Ketofen, Centravet, France), Fucidin cream (Fucidine 2%, Laboratoires Leo, France) and iodine solution (BetadineDermique 10%, MedaPharma, France). All rats followed a post-operative antibiotic treatment (Duphamox, Fort Dodge, France). Behavioral experiments were initiated 21 days post-surgery to allow recovery of the animals from surgery.

3.2. Tissue/Macro-Electrode Interface Characterization

In order to characterize the tissue/macro-electrode interface in the LFP band and develop the model, data were obtained from a bench top *in vitro* and *in vivo* setup. The setup and measurement details are described in detail elsewhere [29]. Briefly, Figure 4a presents the setup based on a voltage divider formed by a reference resistor and the electrode. In order to mimic biological conditions, the generated stimulus amplitude was in the range of LFPs. Preliminary experiments with a commercial recording setup led to identification of the maximum LFP amplitude. The commercial recording setup included a Neurolog (Digitimer, UK) acquisition system and a Powerlab (AD Instruments, USA) interface. The NEX100 and MS306/SP macro-electrodes were used to record the neuronal signals with COS low noise amplifiers (INA114AP, TI) in both *in vitro* solution (Ovalbumin, Ovatransferrin and Ovomucoid simulating the brain medium) and terminal rodent studies.

Figure 4. Test-bench and *in vivo* setups for the tissue/macro-electrode characterization, the integrated neuronal amplifier (NA) characterization, and the recording of the subthalamic nucleus (STN) neural activity using a macro-electrode. (**a**) Tissue/macro-electrode characterization in anesthetized rat [1]; (**b**) Setup representation for the test-bench and *in vivo* experiments [2]; (**c**) Schematic representation of the noise characterization setup (top) and its linear uncorrelated noise model (bottom) [3]; (**d**) The photograph shows the *in vivo* local field potentials (LFP) recording setup with an awake and moving animal, real-time oscilloscope display (MSO6034A) and spectrum analyzer (HP89410A) [4].

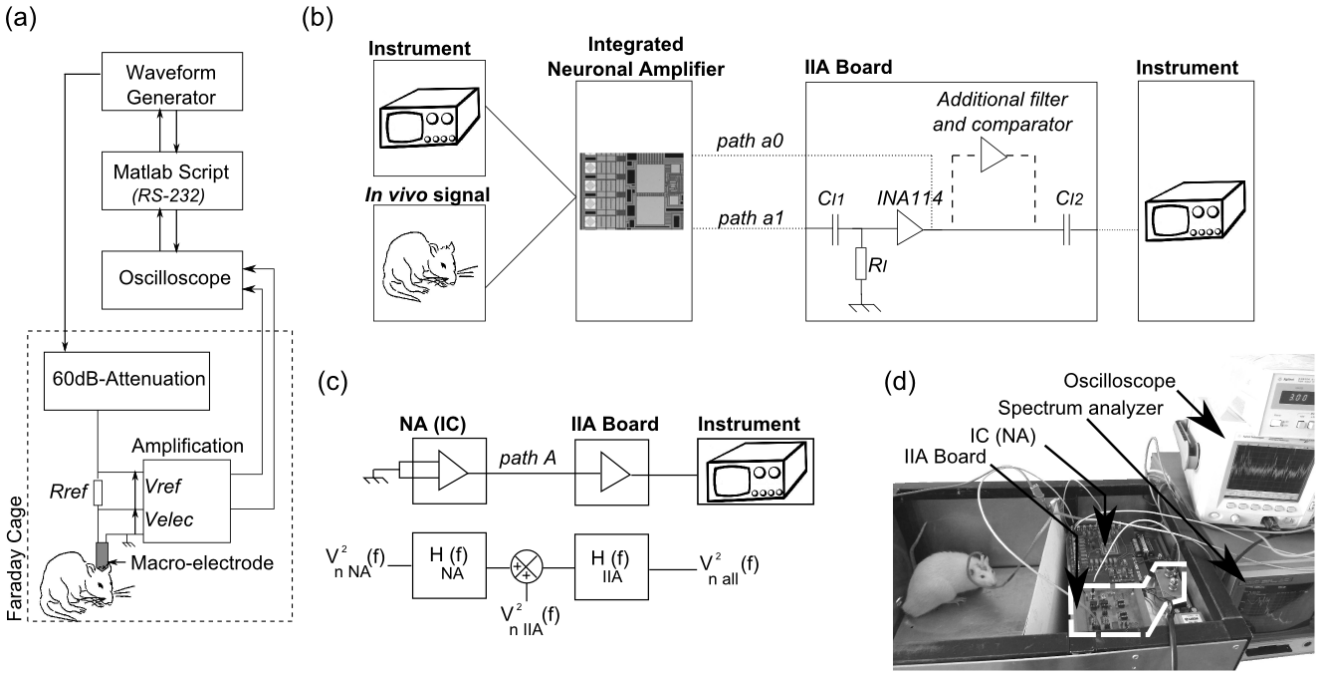

Notes: [1.] The macro-electrode was used to stimulate the STN with a low amplitude signal from a waveform generator and an attenuator. The voltage divider circuit in the amplifier was formed by the reference resistor R_{ref} and the macro-electrode impedance. The V_{ref} and V_{elec} divider circuit output voltages were amplified to be measured with an oscilloscope. Input amplitude and frequency parameters, as well as output voltages were controlled and saved with a custom Matlab script; [2.] The NA input connection depends on the measurement needed. The input was shorted or connected to instrumentation (for electrical characterization or test-bench validation), or connected to the implanted electrode (for *in vivo* experimental validation). The NA output was connected to an adaptation IIA board either without amplification (path a0) or after additional amplification (path a1). For the second amplification stage, commercial-off-the-shelf components, a 40dB low noise INA114 amplifier, and polarization capacitors C_{I1}, C_{I2} and a resistor R_I were used. Unless stated otherwise, C_{I1} = C_{I2} = 150nF and R_I = 1MΩ. The amplified signal was captured directly for the *in vivo* experimental validation or processed further using commercial instrumentation for test-bench validation. The additional circuitry (dashed line) consisted of an additional filter (16 dB-gain, 0.02–16 kHz bandwidth) and a threshold comparator based on a TL082CP amplifier operational amplifier. [3.] The noise model includes the noise power spectral density $v_n^2(f)$ of the NA on the integrated circuit and that on the IIA board or the overall chain and their transfer functions $H(f)$. The setup used a Faraday cage and all device grounds and NA inputs were shorted. Measurements were recorded on a computer through a GPIB connection and controlled using Labview ™ software. [4.] The *in vivo* signal was recorded by a macro-electrode (NEX100, Phymep, France) and was connected to the integrated NA by a ground shielded wire, followed by the IIA board (path a1) and by instrumentation for recording or analyzing purposes (spectrum analyzer, oscilloscope, others). A single electric ground point was used for the overall setup.

3.3. Neuronal Amplifier Electrical Characterization

Figure 4b presents the setups for bench testing and *in vivo* experiments. For electrical characterization, the integrated NA was followed by an adaptation board (IIA), and by commercial instruments (e.g., oscilloscope). Because the signal range is too small to be measured with our instruments (at least 2 μV for the spectrum analyzer, 2 mV for the oscilloscope), a second low noise 40 dB amplification stage was required, and was designed with COS components on the IIA board. Passive component sizing relied on a trade-off between DC rejection and noise attenuation. The polarization capacitor C_{I2} on the IIA board was required for DC match with the following display and analysis instrumentation. The paths a0 and a1 were used respectively for frequency response and power spectral density (PSD) $v_n^2(f)$ characterizations. Eight NA samples on eight chips were characterized. The overall measurement bandwidth was divided into two bands to improve the measurement resolution: 0.5–500 Hz and 0.1–10 kHz. The bandwidth resolution was defined as the tenth of the lowest frequency in those bands. The low frequency characterization down to DC (in the order of milli-hertz) was performed with an HP89410A spectrum analyzer. In order to measure the expected low cut-off frequency (1 Hz) for the frequency response characterization, a high value of C_{I2} (6.8 μF) was used.

Figure 4c describes the noise measurement setup and its linear noise model. The IIA board was needed because the spectrum analyzer noise was higher than the NA output noise. First, we measured the overall amplification system noise PSD $v_{n\,all}^2(f)$ (with NA and IIA board connected, and with NA inputs grounded), then we measured the IIA board noise PSD $v_{n\,IIA}^2(f)$ (without NA, and with IIA inputs grounded). Assuming that each contribution to noise (boards and instruments) is uncorrelated, the NA noise PSD $v_{n\,NA}^2(f)$ is defined as in (4). Integration of discrete measured data lead to estimates of the equivalent input-referred noise over the measurement bandwidth $\overline{v_{n\,NA}^2(f)}$ as defined in Equation (5).

$$v_{n\,NA}^2(f) = \frac{v_{n\,all}^2(f)}{(H_{NA}^2(f).H_{IIA}^2(f))} - \frac{v_{n\,IIA}^2(f)}{H_{IIA}^2(f)} \tag{4}$$

$$\overline{v_{n\,NA}^2(f)} = \sqrt{\sum_{fmin}^{fmax} v_{n\,NA}^2(f)\,.\Delta f} \tag{5}$$

The figure of merit noise efficiency factor (NEF) introduced in [30] has been widely used in the neuronal amplifier designer community since Harrison used it to present his topology [20], and is defined in (6).

$$NEF = \overline{v_{n\,NA}^2(f)}.\sqrt{\frac{2.I_{tot}}{\pi.U_t.4kT.BW}} \tag{6}$$

with BW the NA band (Hz); $\overline{v_{n\,NA}^2(f)}$ the input referred noise (V_{RMS}) usually integrated on the BW band; I_{tot} the total supply current (A); U_t the thermal voltage; k the Boltzmann constant, and T the temperature (300.15 K).

3.4. Neuronal Amplifier Validation with Synthesized Bio-Signals

To illustrate the ability of the integrated NA to record spike signals, we used a test-bench setup with synthesized waveforms as NA input signals. Synthesized waveforms generated by a waveform generator consisted of the superposition of a 500Hz-sinusoid wave (SW) on peak-to-peak amplitude-controlled noise. Four data sets were generated, one with no noise and three with different noise levels. The signal-to-noise ratio (SNR) is defined as the peak amplitude ratio of the SW signal and the noise.

For this first test-bench validation, the waveform data were loaded into a waveform generator (Agilent 33250A, Agilent Producer, Santa Clara, CA, USA), and the generator output was attenuated using two 30dB attenuators (Agilent 8493B, Agilent Producer, Santa Clara, CA, USA) resulting in a SW signal with a 100 μVpp amplitude for input to the NA. This input signal was amplified and filtered with the integrated NA, a second amplification stage and an additional filter (dashed line, Figure 4b). An operational amplifier comparator (TL082CP) was used as a simple threshold comparator to demonstrate that the recording system SNR did not corrupt the low amplitude sine waves.

The three reference SNR ratios were measured at the waveform generator (*i.e.*, before attenuation), at 3.0 V/V, 2.2 V/V and 1.9 V/V. For each of the four data sets, the SNR results were averaged over 70 measurements at the waveform generator and additional filter outputs.

3.5. Neuronal Amplifier Validation with Awake Rodent Experiments

We used the integrated NA *in vivo* neural recording experiments on awake rodents to verify operation of the circuit when connected *in situ*. Figure 4d presents the *in vivo* setup used in this study. This was a modified version of that used in a preliminary study with an analog programmable circuit (instead of this integrated circuit) [31]. The NA records the raw signal between one of the two contacts of the NEX100 macro-electrode and the ground connected under the skull of the animal. The path a1 referred to in Figure 4b was used for *in vivo* low amplitude signal measurement and power spectral density analysis. The same power spectral density measurement method described for the noise characterization was used for *in vivo* experiments.

4. Results

4.1. Tissue/Electrode Interface Characterization

First, we conducted preliminary experiments with a commercial recording setup. We measured LFP signals of an awake rat with a maximum amplitude of 700 μV using a concentric bipolar NEX100 macro-electrode. The amplitude of the neuronal background activity was determined, on a deeply anesthetized rat, to be 10 μV. These measures confirmed the data provided in the literature and gave us a basis to conduct the *in vivo* tissue/electrode interface characterization.

Figure 5 shows *in vivo* measures of the magnitude of the NEX100 electrode impedance *versus* different levels of voltage stimulus over the LFP band. Randle's model was used in which the electrode is approximated as a resistance R_S followed by a parallel capacitor C_e with resistor R_P. Below

~20 Hz, the electrical behavior of this macro-electrode is capacitive. Above ~20Hz, it is equivalent to a resistor.

Figure 5. Impedance magnitude of the NEX100 macro-electrode *versus* frequency in the LFP band while the electrode is implanted into an anesthetized rat's STN. Different voltage amplitudes have been applied, from 300–700 µV. Maxima and minima impedance curves are represented by the dotted lines and the average impedance curve by the bold line.

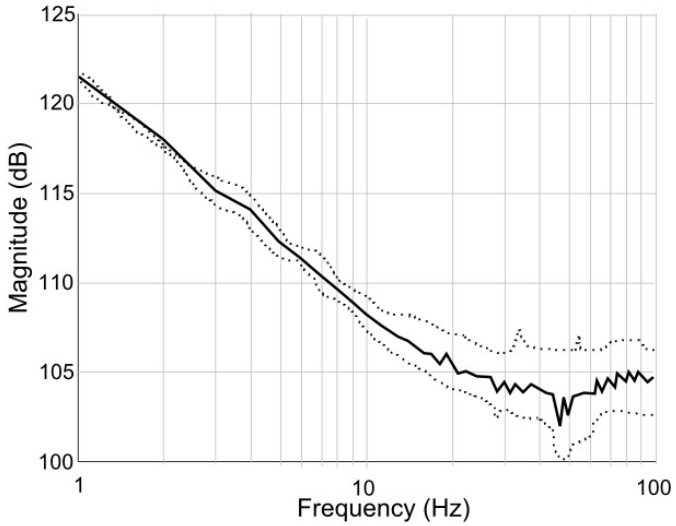

Table 2 compares the measured values for Randle's model of NEX100 and MS360 macro-electrodes with two other electrodes: the Medtronic 3387 DBS electrode and a multi-electrode array (using micro-electrodes) [10,32]. For an acutely implanted electrode, the electrode impedance in the LFP band was approximated by a 34nF-C_e capacitance.

Table 2. Extracted Values of the Electrode Randle's Model Parameter.

Electrode	C_e (F)	R_P (Ohm)	R_S (Ohm)
NEX100 (*in vivo*)	34 nF	>4.68 MΩ	67.8 kΩ
MS306/SP (*in vivo*)	90 nF	>552 kΩ	119 kΩ
NEX100 (*in vitro*)	22.7 nF	>7 MΩ	119 kΩ
MS306/SP (*in vitro*)	17 nF	>4.7 MΩ	<95.5 kΩ
NEX100 (5 months)	74 nF	>2.2 MΩ	113 kΩ
Medtronic 3387 [10]	10 µF	2–5 kΩ	1–500 Ω
Multielectrode array [32]	12 pF	6 TΩ	2–5 kΩ

4.2. Neuronal Amplifier Electrical Characterization

In this section, we present the measurement results for the frequency, noise and power neuronal amplifier performances that meet the required NA specification for future use in a closed-loop implanted neuroprosthesis prototype.

Figure 6 presents the neuronal amplifier frequency response. Figure 6a presents the low cut-off frequency f_{low} measure, which is lower than expected (41.2 mHz *vs.*1 Hz). Figure 6b presents the overall bandwidth of the neuronal amplifier for three different current bias levels. As expected, the

high cut-off frequency f_{high} is tuned by the bias current I_{bias}, as the f_{high} definition in Equation (2) is linear with the transconductance G_m, and itself, linearly dependent on I_{bias} since the input differential transistors are in weak inversion.

Figure 6. Frequency response of the low gain low noise neuronal amplifier. (**a**) Low cut-off frequency f_{low} measure with I_{bias} = 892 nA and C_{I1} = C_{I2} = 6.8 µF; (**b**) High cut-off frequency f_{high} measure with three operational transconductance amplifier biasing currents I_{bias} (from top curve to bottom curve: 892 nA, 523 nA and 334 nA) and IIA board polarization capacitors C_{I1} = C_{I2} = 150 nF.

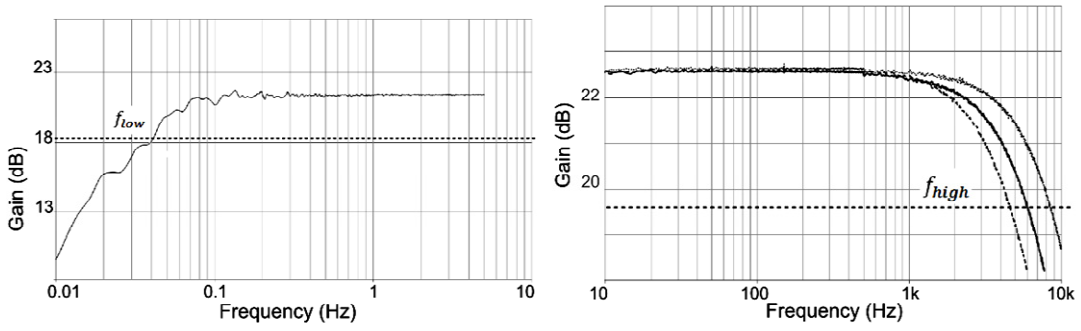

(**a**) (**b**)

Table 3 reports the mean and standard deviations of the NA gain and high cut-off frequency averages for Monte Carlo simulation (300 iterations, process and mismatch variations) and measurements (8 chips from the same fabrication run). The measured standard deviations are smaller than the simulated ones.

Table 3. Performances of the neuronal amplifier.

Parameter	Monte Carlo	Measure
Gain (dB)	21.37 ± 3.94	22.53 ± 0.18
High cut-off frequency(kHz)	13.25 ± 4.13	8.60 ± 2.95

The noise characterization and *in vitro* and *in vivo* measurements performed on an awake animal are illustrated in Figure 7. Figure 7a (bottom curve) plots the NA input-referred noise density *vs.* frequency. To be easily compared with *in vivo* LFP measurements, the input-referred noise is plotted on the 1–500 Hz band only. From this noise figure, we extract the corner frequency f'_{corner} of 39 Hz for the NA and IIA board (path a0, Figure 4b). Because of the IIA board polarization (*i.e.* an equivalent low cut-off frequency of 1 Hz, cf. methods) and according to Equation (3), we conclude that this value gives a maximum limit for the neuronal amplifier's intrinsic f_{corner}. As a consequence, the resultant NA input-referred noise $\overline{v_{n\,NA}^2(f)}$ is also a maximum value, and was found to be 3.99 μV_{RMS} over 1–10 kHz. Figure 7b illustrates the amplified input-referred *in vivo* signal.

Table 4 summarizes measured performances of neuronal amplifiers from the literature based on [20]. We selected NA measured performances that present a noise characterization computed at low frequencies with a maximal low frequency of 10 Hz [17–19,33–37]. This is not the case in most neuronal amplifiers presented in the literature due to the necessary measurement time and effort. The first part of Table 4 presents fabricated circuits meeting the following criteria: they use a 0.35 µm

CMOS process; the low cut-off frequency f_{low} is inferior to 10 Hz and the NA has a bandwidth that covers LFP and spike bands. The second part of Table 4 presents some of the latest neuronal amplifiers (period 2009–2013) that are built using other technologies.

Table 4. Review of performance measures of neuronal amplifiers.

Process (µm)		Gain (dB)	Spectrum (Hz)	$\overline{v_{n_{NA}}^2(f)}$ [BW] (μV_{RMS}, Hz)	NEF	Power/Area (µW/ mm$^{2)}$
0.35	This	22.53	41.2 mHz–8.6 kHz	3.99 [1–10 kHz]	2.04	6.73/0.15
	[17]	46–74	0.1–10 kHz	13.0 [10–10 kHz]	3.53	1.65/0.05
	[18]	34	2.6–6.2 kHz	1.90 [1–6 kHz]	5.10	66/N/A
	[33]	33	10–5 kHz	6.08 [10–5 kHz]	5.55	8.4/0.02
0.13	[34]	37	5–7 kHz	5.5 [NA–7 kHz]	2.58	1.5/N/A
0.13	[35]	40	0.05–10.5 kHz	2.2 [0.1–105 kHz]	2.90	12.1/0.072
0.18	[19]	39.4	10–7.2 kHz	3.5 [10–100 kHz]	3.35	7.92/0.0625
1.5	[36]	80	0.5–10 kHz	3.12 [0.5–50 kHz]	13.80	300/N/A
0.5	[37]	39.6	0.2–8.2 kHz	1.94 [0.5–50 kHz]	2.90	40.1/N/A

Figure 7. Noise characterization, *in vitro* and *in vivo* measurements performed on an awake animal. (**a**) Power spectral density measurements, with V_{pol} = 775 mV, I_{bias} = 1.08 µA: (top curve) *in vivo* input-referred signal density (bottom curve) input-referred neuronal amplifier noise density of the neuronal amplifier; (**b**) Example of an oscilloscope display of the input-referred *in vivo* signal while amplified by the 20 dB neuronal amplifier and the 40dB IIA board commercial amplifier.

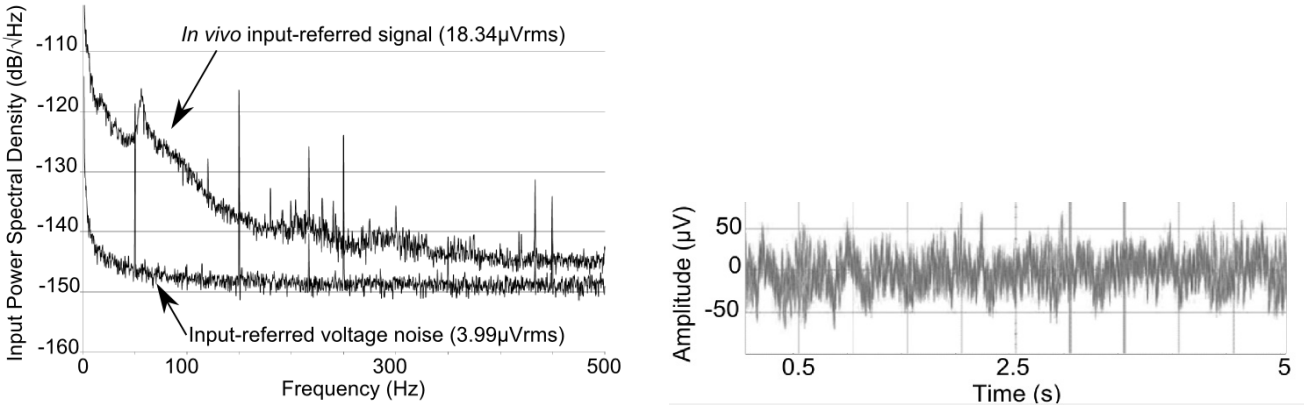

(**a**) (**b**)

4.3. Neuronal Amplifier Validation: Test-Bench Experiments

Figure 8 illustrates the ability of the integrated NA to record spike signals generated using a waveform generator. Table 5 presents SNR measurements at the waveform generator output (input to the NA) and at the recording system (NA) output. When no noise was added on the loaded SW signal, a 2.9 V/V maximum SNR was measured from the recording system. When noise was added on the loaded SW signal, the recording system SNR was close to the input SNR, with constant standard deviation for different noise levels. Figure 8a illustrates a spike output waveform from the generator with added noise while Figure 8b shows the ability to record this activity and identify spikes using a

comparator. The overall gain for the recording system was set at 76 dB (Figure 4b: integrated low noise 20 dB amplifier, INA board second 40dB amplifier, and a 16 dB filter).

Table 5. Spike recording ability of the neuronal amplifier: measured SNR Comparison.

Noise level	Waveform Generator	Recording Output
No noise wave	20.4 V/V ± 4.0%	2.9 V/V ± 7.2%
Noise level #1	3.0 V/V ± 2.1%	2.2 V/V ± 6.4%
Noise level #2	2.2 V/V ± 1.6%	2.0 V/V ± 6.5%
Noise level #3	1.9 V/V ± 2.6%	1.7 V/V ± 6.8%

Figure 8. Test-bench validation measurement example of the neuronal amplifier spike recording ability. (**a**) Waveform generator output with noise level #2 (Table 5); (**b**) (top curve) Output signal of the recording system; spike detection threshold was set at −1.5 V (horizontal line); (bottom curve) comparator output with offset for readability.

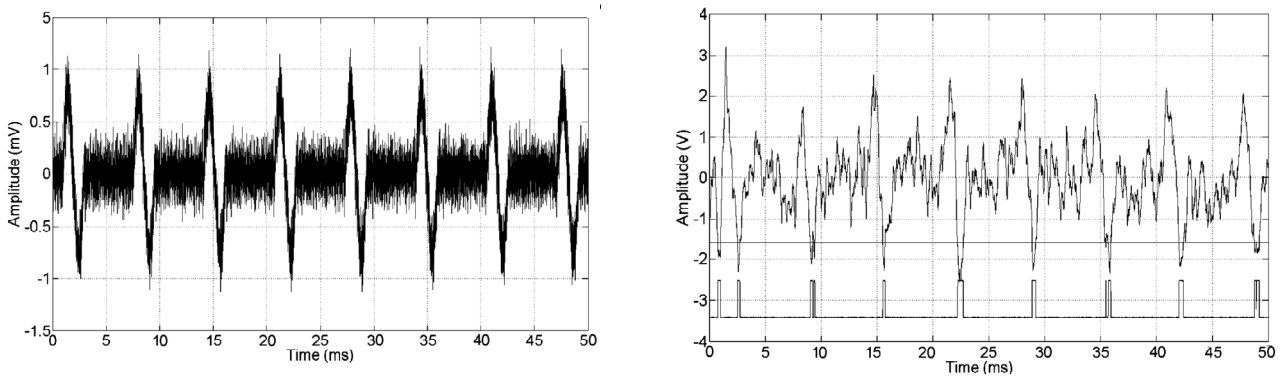

(**a**) (**b**)

4.4. Neuronal Amplifier Validation: Awake Rodents Experiments

After the NA characterization, we conducted several series of *in vivo* measurements to validate the device *in situ*. Our long term goal is to demonstrate that our system can be used for *in vivo* experiments of LFP recording with awake and moving rats.

The *in vivo* power spectral density was measured and was referred to the NA input (Figure 7a, top curve). It is one example among the four measurements made on different days. Animal condition (deeply anesthetized or awake) LFP recording were similar (not shown). *In vivo* input-referred measured PSD was 18.34 μV_{RMS}, integrated on 1–10 kHz.

The NEX100 is a macro-electrode (100 kΩ at 1 kHz); therefore mostly LFPs could be recorded and one oscilloscope hardcopy (Figure 7b) is shown. If the neuronal amplifier output is filtered by a 00 Hz low-pass filter, it provides the same shape as the output of the NA (not shown). The *in vivo* input-referred signal amplitude was 100 μVpp. These results were confirmed in experiments performed on four different animals and over an average of four consecutive hours.

5. Discussion

In this paper, we present an integrated neuronal amplifier with low noise, area and power performance along with a low gain to prevent saturation by the stimulation artifact. We present the full

NA design methodology that meets desired specifications. The ability of the NA to perform spike and LFP recording is illustrated using a test-bench setup. Finally, the circuit's functionality is validated in *in vivo* experiments.

5.1. Tissue/Electrode Interface Characterization

We designed a setup to characterize the tissue/macro-electrode interface using an electrical model by appropriate stimulation of the deep brain subthalamic nucleus region with a small macro-electrode. The stimulation amplitude was chosen to reflect those observed under recording conditions. Indeed, high stimulation amplitude could lead to non-linear effects, which would not reflect the *in vivo* recording conditions. Dispersion of the different measures *versus* the stimulation voltage level (Figure 5) is not significant (less than 2%): these measures suggest a linear model. This confirms the relevance of Randle's linear model for the tissue/macro-electrode model in the LFP band. The impedance characteristics for NEX100 and MS306/SP (Table 1) are similar, which is not surprising given their similar geometrical characteristics. This comparison proves the robustness of the characterization setup. The extracted values from *in vitro* measurements are under-estimated compared to those from *in vivo* studies, suggesting the need for an *in situ* characterization. The characterization of the tissue/macro-electrode interface provides guidelines for the impedance matching between the tissue/macro-electrode interface and the NA, which was addressed by appropriate component sizing in our NA design.

5.2. Neuronal Amplifier Topology

The NA topology addresses the required specifications and meets changes in the biological system input dynamics. Because we are also interested in determining if analog linear processing of the recorded signal could generate a stimulation signal, the heterodyning method is not used.

The front-end design should then consider the electrode DC level and its drift, which are classical NA issues that can result in output saturation. Various techniques have been described [7,38] to eliminate this DC component: high-pass filtering (blocking or subtracting low frequencies), intrinsic low gain at low frequency, stabilization, chopper modulation or offset cancelling. The NA topology presented by Harrison in [20] is one of the most popular for various recording applications (electroencephalogram, electrocardiogram, deep brain recordings with *in vivo* multielectrode array, e.g., [22,39]) because of its low noise and potential low power/area consumptions. The DC level is handled with high-pass filtering with this topology. We chose to use this NA topology and adapt the sizing of the components to meet our challenging specifications regarding the noise, gain and power/area consumptions. We used transistors in moderate and strong inversion to meet noise and power specifications.

5.3. Neuronal Amplifier Performances

Frequency and noise responses are some of the critical specifications for the NA. As shown in Figure 6b, the first frequency response parameter of interest is the low cut-off frequency value. The measured frequency is lower than the simulated value. This can be explained by discrepancies in the

model of the lateral PNP in the 0.35 μm CMOS process design kit which overestimates the cut-off frequencies. This was also observed in the original design [20] with the AMI 1.35μm CMOS process. Moreover, we demonstrated in an awake rat experiment (see following sub-section) that the f_{low} limited change has no impact on the proper functioning of our design.

Mismatch in the circuit fabrication process and parasitic capacitors may be responsible for the difference between simulated and measured performances of the gain and the high cut-off frequency f_{high}. Variation in f_{high} will have little impact on spike recording because this frequency can be chosen in the 5–10 kHz band [14,15] and can still be tuned together with the NA transconductance G_m (I_{bias}) with Equation (2).

Even with a low amplification gain, the NA noise and power/area performances are reasonable compared to that of other high gain amplifiers with the same topology [17–19,33–37]. Moreover, we achieve the best NEF among all technology process designs. Note that a recent paper [18] has presented the same recording circuit strategy in an integrated circuit but no bandwidth characterization over the continuous LFP and spike band and with no *in vivo* LFP recordings presented. Moreover, their NA gain was set at a value (50V/V) that may be too high to be used in a closed-loop system such as that presented in the Kent and Grill study [8].

5.4. Neuronal Amplifier Validation: Test-Bench and Awake Rodent Experiments

Additional test-bench experiments illustrate the ability of the NA to record spikes with several SNRs. The true SNR at the NA input cannot be determined because the NA input can also record uncontrolled external thermal noise. However, this demonstration shows that the output SNR decreased in proportion to the input SNR, and with a low standard variation (Table 5). The detection rate was acceptable because we used a simple threshold method. This extension of the NA bandwidth over the spike band provides the opportunity for a large variety of closed-loop paradigm validations.

Because the LFP signal shares many features with the noise signal, the following measurement shows that the *in vivo* recorded signal is indeed an *in vivo* spontaneous neural recording, and not NA intrinsic noise. In Figure 7a, the *in vivo* PSD referred to the NA input (18.34 μV_{RMS}) is compared with the NA input-referred noise (3.99 μV_{RMS}): this demonstrates that our *in vivo* recordings are indeed *in vivo* extracellular brain measurements.

As an example, Figure 7b presents the NA recording output signal amplitude and shape. The NA recordings are equivalent to the LFPs recorded in the same condition using a commercial recording setup. Our NA not only provides similar characteristics but our integrated circuit is also portable because of its small size and operability using a battery source. These successful *in vivo* validations with awake and freely moving rats lead the way for extended investigations of LFP control within a closed-loop system for various applications.

This recording circuit strategy requires careful noise consideration for the cascade of low gain second-order filter amplifier stages in the neuronal amplifier in order to maximize the SNR as defined in Friis formula [40]. A recent manuscript [18] also assesses that such a design is achievable. The recording circuit architecture with the artifact reduction strategy we used has proven successful for *in vivo* recording and stimulation of neuronal activity by [6] in the subthalamic nucleus (STN) of two idiopathic parkinsonian patients, and by [8], in the ventral lateral thalamus of an adult cat, both using

COS components [6,8]. Thus, we believe that this NA is suitable for recording LFPs and spikes for a future implantable closed-loop system using a single electrode.

Acknowledgment

Authors would like to thanks Marion Monnier and Emilie Syed for measurements and *in vivo* experiments help, Florian Kölbl for *in vitro* recordings, as well as Thomas Boraud for highly valuable discussions regarding the *in vivo* experiments and future directions on this project. Finally, the authors would like to thank Amy Starosciak and James Abbas for manuscript review and support during the revision process.

Conflicts of Interest

The authors declare no conflict of interest.

References

1. Eberle, W.; Penders, J.; Yazicioglu, R.F. Closing the Loop for Deep Brain Stimulation Implants Enables Personalized Healthcare for Parkinson's Disease Patients. In Proceedings of the Annual International Conference of the IEEE Engineering in Medicine and Biology Society, MA, USA, 30 Auguest–3 September 2011; pp. 1556–1558.
2. Santaniello, S.; Fiengo, G.; Glielmo, L.; Grill, W.M. Closed-loop control of deep brain stimulation: A simulation study. *IEEE Trans. Neural Syst. Rehabil. Eng*. **2011**, *19*, 19–24.
3. Chung, P.Y.; Sheng, F.L.; Da, W.C.; Yi, C.L.; Fu-Zen, S.; Chao-Hsien, H. A portable wireless online closed-loop seizure controller in freely moving rats. *IEEE Trans. Instrum. Meas.* **2011**, *60*, 513–521.
4. Little, S.; Pogosyan, A.; Kuhn, A.A.; Brown, P. Beta band stability over time correlates with parkinsonian rigidity and bradykinesia. *Exp. Neurol.* **2012**, *236*, 383–388.
5. McLaughlin, M.; Lu, T.; Dimitrijevic, A.; Fan, G.Z. Towards a closed-loop cochlear implant system: Application of embedded monitoring of peripheral and central neural activity. *IEEE Trans. Neural Syst. Rehabil. Eng.* **2012**, *20*, 443–454.
6. Rossi, L.; Foffani, G.; Marceglia, S.; Bracchi, F.; Barbieri, S.; Priori, A. An electronic device for artefact suppression in human local field potential recordings during deep brain stimulation. *J. Neural Eng.* **2007**, *4*, 96–106.
7. Jochum, T.; Denison, T.; Wolf, P. Integrated circuit amplifiers for multi-electrode intracortical recording. *J. Neural Eng.* **2009**, *6*, doi:10.1088/1741-2560/6/1/012001.
8. Kent, A.R.; Grill, W.M. Recording evoked potentials during deep brain stimulation: Development and validation of instrumentation to suppress the stimulus artefact. *J. Neural Eng.* **2012**, *9*, doi:10.1088/1741-2560/9/3/036004.
9. Stanslaski, S.; Afshar, P.; Cong, P.; Giftakis, J.; Stypulkowski, P.; Carlson, D.; Linde, D.; Ullestad, D.; Avestruz, A.; Denison, T. Design and validation of a fully implantable, chronic, closed-loop neuromodulation device with concurrent sensing and stimulation. *IEEE Trans. Neural Syst. Rehabil. Eng.* **2012**, *20*, 410–421.

10. Wei, X.F.; Grill, W.M. Impedance characteristics of deep brain stimulation electrodes *in vitro* and *in vivo*. *J. Neural. Eng.* **2009**, *6*, doi:10.1088/1741-2560/6/4/046008.
11. Lempka, S.F.; Miocinovic, S.M.; Jonson, M.D.; Vitek, J.L.; McIntyre, C.C.; Wei, X.F.; Grill, W.M. *In vivo* impedance spectroscopy of deep brain stimulation electrodes. *J. Neural Eng*. **2009**, *6*, doi:10.1088/1741-2560/6/4/046001.
12. Gubellini, P.; Salin, P.; Kerkerian-Le, G.L.; Baunez, C., Deep brain stimulation in neurological diseases and experimental models: From molecule to complex behavior. *Prog. Neurobiol.* **2009**, *89*, 79–123.
13. Denison, T.; Consoer, K.; Santa, W.; Avestruz, A.T.; Cooley, J.; Kelly, A. A 2uw 100 nv/rthz chopper-stabilized instrumentation amplifier for chronic measurement of neural field potentials. *IEEE J. Solid State Circuits* **2007**, *42*, 2934–2945.
14. Harrison, R.R. A Versatile Integrated Circuit for the Acquisition of Biopotentials. In Proceedings of the IEEE Custom Integrated Circuits Conference, San Jose, CA, USA, 16–19 September 2007; pp. 115–122.
15. Schwartz, A.B.; Cui, X.T.; Weber, D.J.; Moran, D.W. Brain-controlled interfaces: Movement restoration with neural prosthetics. *Neuron* **2006**, *52*, 205–220.
16. Dagtekin, M.; Wentai, L.; Bashirullah, R. A Multi Channel Chopper Modulated Neural Recording System. In Proceedings of the 23rd Annual International Conference of Engineering in Medicine and Biology Society, Istanbul, Turkey, 25–28 October 2001; pp. 757–760.
17. Aziz, J.N.Y.; Genov, R.; Bardakjian, B.L.; Derchansky, M.; Carlen, P.L. Brain-silicon interface for high-resolution *in vitro* neural recording. *IEEE Trans. Biomed. Circuits Syst.* **2007**, *1*, 56–62.
18. Lopez, C.M.; Prodanov, D.; Braeken, D.; Gligorijevic, I.; Eberle, W.; Bartic, C.; Puers, R.; Gielen, G. A multichannel integrated circuit for electrical recording of neural activity, with independent channel programmability. *IEEE Trans. Biomed. Circuits Syst*. **2012**, *6*, 101–110.
19. Majidzadeh, V.; Schmid, A.; Leblebici, Y. Energy efficient low-noise neural recording amplifier with enhanced noise efficiency factor. *IEEE Trans. Biomed. Circuits Syst*. **2011**, *5*, 262–271.
20. Harrison, R.R.; Charles, C. A low-power low-noise CMOS amplifier for neural recording applications. *IEEE J. Solid State Circuits* **2003**, *38*, 958–965.
21. Bai, Q.; Wise, K.D., Single-unit neural recording with active microelectrode arrays. *IEEE Trans. Biomedl. Eng.* **2001**, *48*, 911–920.
22. Heer, F.; Hafizovic, S.; Franks, W.; Blau, A.; Ziegler, C.; Hierlemann, A. cmos microelectrode array for bidirectional interaction with neuronal networks. *IEEE J. Solid State Circuits* **2006**, *41*, 1620–1629.
23. Delbruck, T.; Mead, C.A. Adaptive photoreceptor with wide dynamic range. *IEEE Int. Symp. Circuits Syst.* **1994**, *334*, 339–342.
24. Laker, K.R.; Sansen, W.M.C. *Design of Analog Integrated Circuits and Systems*; Mcgraw-Hill College Division: New York, NY, USA, 1994.
25. Binkley, D.M.; Hopper, C.E.; Tucker, S.D.; Moss, B.C.; Rochelle, J.M.; Foty, D.P. A cad methodology for optimizing transistor current and sizing in analog CMOS design. *IEEE Trans. Comput. Aided Des. Integr. Circuits Syst.* **2003**, *22*, 225–237.
26. Harrison, R.R. The design of integrated circuits to observe brain activity. *Proc. IEEE* **2008**, *96*, 1203–1216.

27. Zbrzeski, A.; Lewis, N.; Syed, E.; Benazzouz, A.; Boraud, T.; Renaud, S. A Tunable Integrated Device for LFP Tracking. In Proceedings of the 26th Conference on Design of Circuits and Integrated systems, Albufeira, Portugal, 16–18 November 2011; pp. 439–442.
28. Paxinos, G.; Watson, C. *The Rat Brain in Stereotaxic Coordinates*; Academic Press: London, UK, 1998.
29. Kolbl, F.; Zbrzeski, A.; Syed, E.; Renaud, S.; Lewis, N. In *in vivo* Electrical Characterization of Deep Brain Electrode and Impact on Bio-Amplifier Design. In Proceedings of the IEEE Biomedical Circuits and Systems Conference, Paphos, Cyprus, 3–5 November 2010; pp. 210–213.
30. Steyaert, M.S.J.; Sansen, W.M.C. A micropower low-noise monolithic instrumentation amplifier for medical purposes. *IEEE J. Solid State Circuits* **1987**, *22*, 1163–1168.
31. Zbrzeski, A.; Hasler, P.; Ko, X.; lbl, F.; Syed, E.; Lewis, N.; Renaud, S. A Programmable Bioamplifier on FPAA for *in vivo* Neural Recording. In Proceedings of the IEEE Biomedical Circuits and Systems Conference, Paphos, Cyprus, 3–5 November 2010; pp. 114–117.
32. Najafi, K.; Wise, K.D. An implantable multielectrode array with on-chip signal processing. *IEEE J. Solid State Circuits* **1986**, *21*, 1035–1044.
33. Shahrokhi, F.; Abdelhalim, K.; Serletis, D.; Carlen, P.L.; Genov, R., The 128-channel fully differential digital integrated neural recording and stimulation interface. *IEEE Trans. Biomed. Circuits Syst*. **2010**, *4*, 149–161.
34. Chaturvedi, V.; Amrutur, B. An area-efficient noise-adaptive neural amplifier in 130 nm cmos technology. *IEEE J. Emerg. Sel. Top. Circuits Syst.* **2011**, *1*, 536–545.
35. Zhang, F.; Holleman, J.; Otis, B.P. Design of ultra-low power biopotential amplifiers for biosignal acquisition applications. *IEEE Trans. Biomed. Circuits Sys.* **2012**, *6*, 344–355.
36. Farshchi, S.; Pesterev, A.; Nuyujukian, P.; Guenterberg, E.; Mody, I.; Judy, J.W. Embedded neural recording with tinyos-based wireless-enabled processor modules. *IEEE Trans. Neural Syst. Rehabil. Eng.* **2010**, *18*, 134–141.
37. Mollazadeh, M.; Murari, K.; Cauwenberghs, G.; Thakor, N. Micropower cmos integrated low-noise amplification, filtering, and digitization of multimodal neuropotentials. *IEEE Trans. Biomed. Circuits Syst.* **2009**, *3*, 1–10.
38. Olsson, R.H., III; Wise, K.D. A three-dimensional neural recording microsystem with implantable data compression circuitry. *IEEE J. Solid. State Circuits* **2005**, *40*, 2796–2804.
39. Yazicioglu, R.F.; Merken, P.; Puers, R.; Van Hoof, C. A 60 µw 60 nv/hz Readout Front-End for Portable Biopotential Acquisition Systems. In Proceedings of the IEEE International Solid-State Circuits Conference, San Francisco, CA, USA, 6–9 February 2006; pp. 109–118.
40. Ziel, A.V.D. *Noise*: *Sources*, *Characterization*, *Measurement*; Prentice-Hall: Upper Saddle River, NJ, USA, 1970.